CHEMISTRY
A EUROPEAN JOURNAL

DOI: 10.1002/chem.200501035

Heteropolynuclear Palladium Complexes with Pyrazolate and Its 3-*tert*-Butyl Derivatives: The Effect of Heterometal Ions on the Rate of Isomerization

Keisuke Umakoshi,* Takashi Kojima, Yasuhiro Arikawa, and Masayoshi Onishi*[a]

Abstract: The heteropolynuclear complexes $[Pd_2M'_2(\mu\text{-pz})_6]$ (M′ = Ag (**1**), Au (**2**); pzH = pyrazole), *HT*-$[Pd_2M'_2(\mu\text{-3-}t\text{Bupz})_6]$ (M′ = Ag (**3a**), Au (**4a**); 3-*t*BupzH = 3-*tert*-butylpyrazole), and *HH*-$[Pd_2Au_2(\mu\text{-3-}t\text{Bupz})_6]$ (**4b**) have been prepared and some of them were structurally characterized. When 3-*tert*-butylpyrazolate was employed as a bridging ligand, two linkage isomers (head-to-tail (*HT*) and head-to-head (*HH*)) arise from the difference in orientation of the substituent groups on the pyrazolate bridges between the two Pd atoms. ^{1}H NMR spectroscopy has been used to identify and to follow the reversible stereochemical rearrangement of the *HH* isomer of $[Pd_2Ag_2(\mu\text{-3-}t\text{Bupz})_6]$ (**3b**) to form the *HT* isomer **3a** in $CDCl_3$ and the *HT* isomer of $[Pd_2Au_2(\mu\text{-3-}t\text{Bupz})_6]$ (**4a**) to form the *HH* isomer **4b** in C_6D_6. Kinetic studies of the reaction have established the rate law to be $-d(HH)/dt = d(HT)/dt = k_2[HH] - k_1[HT]$ for **3b** and $-d(HT)/dt = d(HH)/dt = k_1[HT] - k_2[HH]$ for **4a**, where k_1 and k_2 denote the rate of isomerization from the *HT* to the *HH* isomer and that from the *HH* to the *HT* isomer, respectively. For typical runs at 50 °C in C_6D_6, $k_1 = 13.8 \times 10^{-5}\,s^{-1}$, $k_2 = 18.6 \times 10^{-5}\,s^{-1}$, and $K_{eq} = k_2/k_1 = 1.24$ for **3b**, and $k_1 = 1.26 \times 10^{-5}\,s^{-1}$, $k_2 = 3.52 \times 10^{-5}\,s^{-1}$, and $K_{eq} = k_1/k_2 = 0.36$ for **4a**. Temperature-dependent rate measurements reveal $\Delta H^{\neq}$ and $\Delta S^{\neq}$ to be 100(1) kJ mol^{-1} and 0(3) J mol^{-1} K^{-1} for **3b** and 112(5) kJ mol^{-1} and 20(17) J mol^{-1} K^{-1} for **4a**, respectively. The rate of isomerization is essentially unaffected by the concentration of the complex or by the presence of neutral bridging ligands. These data and observations imply that the isomerization involves an intramolecular exchange process.

Keywords: heterometallic complexes · isomerization · kinetics · N ligands · palladium

Introduction

Polynuclear transition-metal complexes with pyrazoles and/or pyrazolates have been attracting attention because of their versatile structures and properties.[1] Among the various types of structures, pyrazolate and its derivatives are known to favor the formation of cyclic trinuclear complexes such as $[M^I_3(\mu\text{-Rpz})_3]$ (M^I = Cu,[2–4] Ag,[3,5,6] Au;[5,7] RpzH = pyrazole or substituted pyrazoles) and $[M^{II}_3(\mu\text{-Rpz})_6]$ (M^{II} = Pd,[8,9] Pt[9,10]), the structure of the latter being similar to that of palladium(II) acetate $[Pd_3(\mu\text{-OAc})_6]$.[11] The successful partial oxidation of the platinum cyclic trimer $[Pt^{II}_3(\mu\text{-pz})_6]$ has enabled the isolation of $Pt^{II,III,III}_3$ species, and the geometrical and electronic structures of $[Pt_3Br_2(\mu\text{-pz})_6]$ have been elucidated.[12]

The number of heteropolynuclear pyrazolate complexes is also gradually increasing.[9,13,14] Because pyrazole is a weak acid, the reaction conditions and the nature of the central metal ions help to determine whether coordinated pyrazoles exist as the protonated form (pyrazoles) or the deprotonated form (pyrazolates). The protons in coordinated pyrazoles often participate in intra- or intermolecular hydrogen bonding, and they can be replaced by metal ions such as Cu^I, Ag^I, and Au^I to give heterometallic polynuclear complexes.[9,13,14] In the formation of heteropolynuclear complexes, the precursors with intramolecular hydrogen bonding, such as $[Pd_2(\mu\text{-Rpz})_2(Rpz)_2(RpzH)_2]$ (R = 3-*tert*-butyl, 3,5-dimethyl), give tetranuclear complexes of the $Pd_2M'_2$ type (M′ = Cu, Ag, Au),[9,14] while those with intermolecular hydrogen bonding, such as $[\{M(Rpz)_2(RpzH)_2\}_2]$ (M = Pd, Pt; R = H, 3,5-dimethyl), afford hexanuclear complexes of the $M_2M'_4$ type (M′ = Cu, Ag).[9,13] The use of asymmetrical pyrazolate ligands further adds to the possibility of formation of geometrical isomers for each heteropolynuclear complex. A detailed study of the reaction of *HT*-$[Pd_2(\mu\text{-3-}$

[a] Prof. Dr. K. Umakoshi, T. Kojima, Dr. Y. Arikawa, Prof. Dr. M. Onishi
Department of Applied Chemistry, Faculty of Engineering
Nagasaki University, Bunkyo-machi, Nagasaki 852-8521 (Japan)
Fax: (+81) 95-819-2672
E-mail: kumks@net.nagasaki-u.ac.jp
onishi@net.nagasaki-u.ac.jp

Supporting Information for this article is available on the WWW under http://www.chemeurj.org/ or from the author.

*t*Bupz)$_2$(3-*t*Bupz)$_2$(3-*t*BupzH)$_2$] with Ag^I and an Au^I complex have enabled us to isolate two linkage isomers of tetranuclear complexes, namely the head-to-head (*HH*) and the head-to-tail (*HT*) isomer (Scheme 1). These arise from the difference in the orientation of the substituents on the pyrazolate bridges between the two Pd atoms. The proportion of each linkage isomer was found to be dependent on the synthetic route. Because a facile stereochemical rearrangement of the linkage isomers was observed at elevated temperature, it was followed by ^{1}H NMR spectroscopy. Although a similar stereochemical rearrangement has been observed for the *HH* isomer of [Pt$^{II}_2$(en)$_2$(α-pyridonate)$_2$](NO$_3$)$_2$,[15] this is the first observation of an isomerization occurring selectively at the bridges between Pd atoms rather than any of the other six possible bridges (including the bridges between Pd and Ag or Au). The most remarkable feature of the isomerization in this system is that the Ag^I or Au^I ions affect the rate, whereas the ligands at the Pd···Ag or Pd···Au bridges apparently do not participate in the isomerization reaction. These findings also prompted us to investigate the formation of heteropolynuclear complexes with nonsubstituted pyrazole. We found in this case that mononuclear Pd^{II} complexes with neutral pyrazoles or solvent molecules can be precursors of Pd$_2$M′$_2$ complexes.

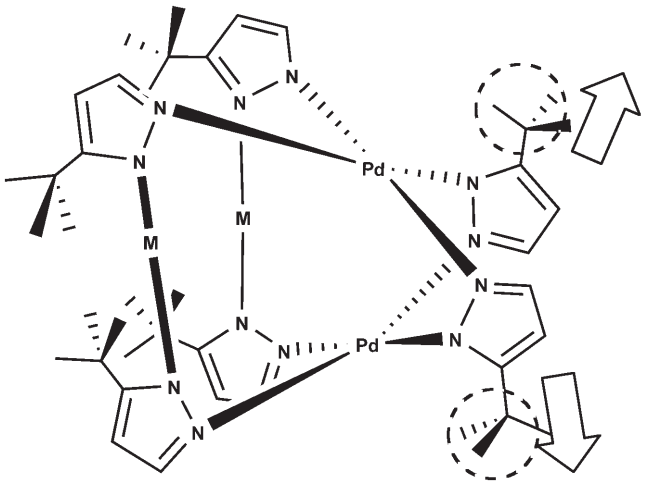

HT isomer

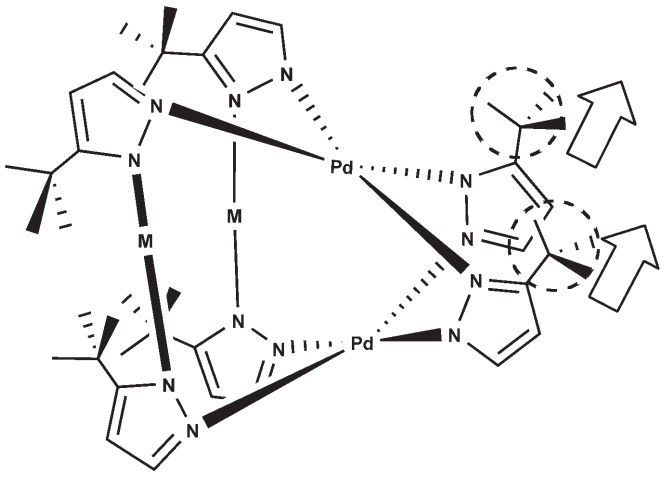

HH isomer

Scheme 1. Schematic representation of linkage isomers.

Herein, we report the synthesis and structural characterization of pyrazolate-bridged heteropolynuclear complexes and the linkage isomers arising from the use of asymmetrically substituted pyrazolate (3-*tert*-butylpyrazolate). The results of the kinetic study on the isomerization of these linkage isomers (*HT* and *HH* isomers) are also presented.

Results and Discussion

Preparation of complexes: Substituted pyrazoles such as 3-*tert*-butylpyrazole (3-*t*BupzH) and 3,5-dimethylpyrazole (dmpzH) are known to form either a dinuclear Pd^{II} complex with intramolecular hydrogen bonding, in which some of the pyrazolate ligands act as bridging ligands,[9,14] or a dimer of mononuclear Pd^{II} complexes with intermolecular hydrogen bonding, in which both pyrazolate and pyrazole ligands coordinate to the Pd^{II} ion in a monodentate fashion.[13] Pyrazole without any substituent groups (pzH), however, forms a cyclic trinuclear Pd^{II} complex, [Pd$_3$(μ-pz)$_6$], under basic conditions and a mononuclear Pd^{II} complex with four neutral pyrazole ligands, [Pd(pzH)$_4$]Cl$_2$, under acidic conditions. The product formed under basic conditions contrasts with the case of Pt^{II}, which forms a dimer of mononuclear complexes with intermolecular hydrogen bonding, [{Pt(pz)$_2$-(pzH)$_2$}$_2$].[9,16] There are two different methods for the preparation of the heteropolynuclear Pd^{II} complexes [Pd$_2$M′$_2$(μ-pz)$_6$] (M′ = Ag (**1**), Au (**2**)): one involves the reaction of isolated [Pd(pzH)$_4$]Cl$_2$ with an Ag^I salt or Au^I complex in the presence of Et$_3$N (method A), and the other involves the reaction of pzH with the mixture of Pd^{II} and Ag^I ions generated by the addition of an excess of Ag^I salt to a solution containing [PdCl$_2$(CH$_3$CN)$_2$] and Et$_3$N (method B) (Scheme 2).

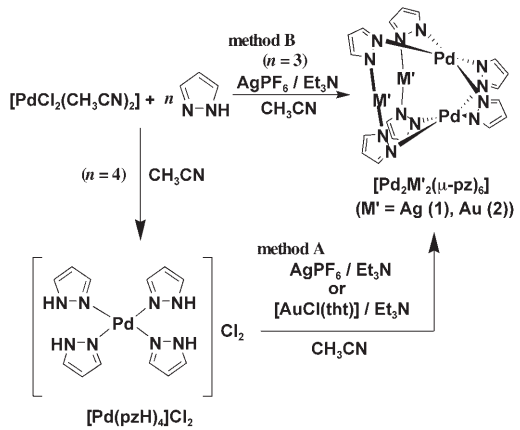

Scheme 2. Preparative methods for [Pd$_2$M′$_2$(μ-pz)$_6$] (M′ = Ag, Au).

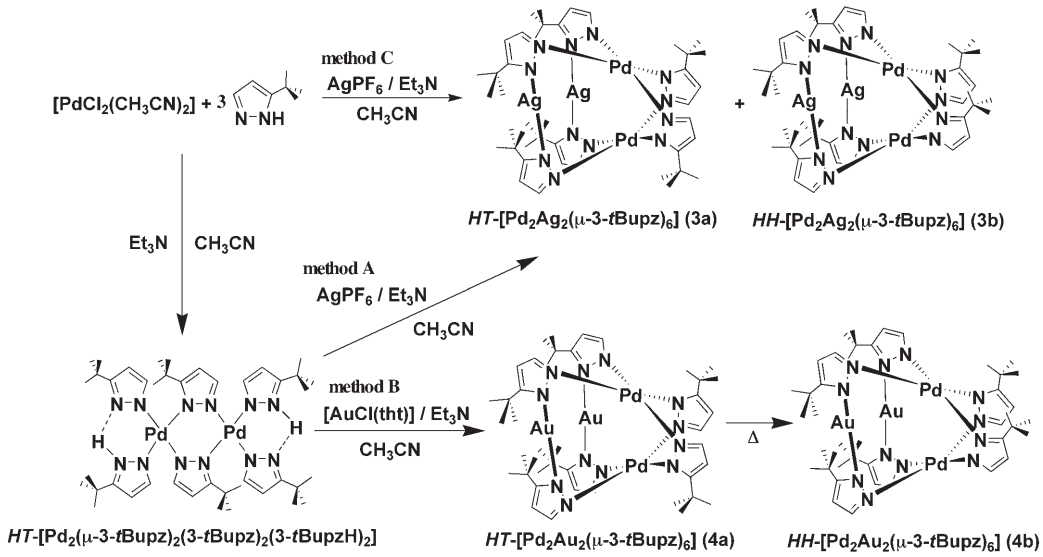

Scheme 3. Preparative methods for $[Pd_2M'_2(\mu\text{-}3\text{-}t\text{Bupz})_6]$ (M′ = Ag, Au).

The substitution of an Au^I complex for the Ag^I salt in the latter method gave a complicated reaction mixture. The total yield of **1** based on $[PdCl_2(CH_3CN)_2]$ in the former method is 48%, which is higher than that (20%) obtained with the latter method.

The synthesis of heteropolynuclear complexes with similar structures to **1** and **2** but containing 3-*t*Bupz mainly gave two geometrical isomers among the several possible ones. When intramolecularly hydrogen-bonded *HT*-$[Pd_2(\mu\text{-}3\text{-}t\text{Bupz})_2(3\text{-}t\text{Bupz})_2(3\text{-}t\text{BupzH})_2]$ was employed as starting material, the reaction with Au^I complex gave *HT*-$[Pd_2Au_2(\mu\text{-}3\text{-}t\text{Bupz})_6]$ (**4a**) selectively in 75% yield (Scheme 3). The absence of the *HH* isomer (**4b**) was confirmed by recording a ^{1}H NMR spectrum just after completion of the reaction. However, it was difficult to isolate the pure *HT* isomer of the silver analogue **3a** even by treating *HT*-$[Pd_2(\mu\text{-}3\text{-}t\text{Bupz})_2(3\text{-}t\text{Bupz})_2(3\text{-}t\text{BupzH})_2]$ with a Ag^I salt. The ^{1}H NMR spectrum of the reaction mixture recorded just after completion of the reaction revealed that the ratio of the *HT* and *HH* isomers **3a** and **3b**, respectively, was 10:1. The apparent formation of **3b** in the reaction can be attributed to the isomerization of **3a** to **3b** (vide infra). Although we have reported previously that the reaction of *HT*-$[Pd_2(\mu\text{-}3\text{-}t\text{Bupz})_2(3\text{-}t\text{Bupz})_2(3\text{-}t\text{BupzH})_2]$ with a Ag^I salt gives the *HH* isomer of $[Pd_2Ag_2(\mu\text{-}3\text{-}t\text{Bupz})_6]$ (**3b**),[9] it is now clear that the main product of this reaction is the *HT* isomer **3a**. It is also obvious that the successful isolation of **3b** as a pure product from the reaction of 3-*t*Bupz with the mixture of Pd^{II} and Ag^I ions is due to the lower solubility of **3b** than **3a**. The ^{1}H NMR spectrum of the reaction mixture revealed that the reaction mixture in method C (Scheme 3) contains almost the same amount of **3a** and **3b** just after the reaction has finished. An attempt to prepare $[Pd_2Au_2(\mu\text{-}3\text{-}t\text{Bupz})_6]$ by the reaction of 3-*t*BupzH with a mixture of $[PdCl_2(CH_3CN)_2]$ and [AuCl(tht)] in the presence of Et_3N was unsuccessful and gave a complicated mixture of products.

Crystal structures: X-ray structural analyses were performed for single crystals of **1**, **2**, **4a**, and **4b**. Depending on the synthetic procedure, the Pd/Ag complex bridged by nonsubstituted pyrazolate ligands, $[Pd_2Ag_2(\mu\text{-}pz)_6]$ (**1**; Figure 1), afforded two different crystals, one with and one without solvent of crystallization. The crystals obtained by following method A in Scheme 2 contain three acetonitrile molecules per complex molecule. No intermolecular metal–metal interaction is seen in this crystal structure. The complex molecule has an idealized C_{2v} symmetry. The Pd^{II} centers are square planar and the Ag^I centers linear, with N-Ag-N angles of

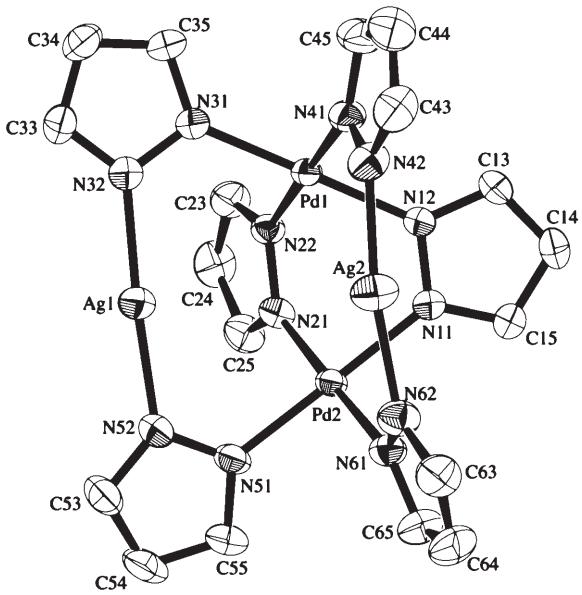

Figure 1. Molecular structure of $[Pd_2Ag_2(\mu\text{-}pz)_6]$ (**1**) with the atom numbering scheme (50% probability ellipsoids).

174.5(1)° and 167.5(1)°. The intermetallic distances are 3.4341(3) Å for Pd1···Pd2 and 3.44–3.47 Å for Pd···Ag (Table 1). The Ag–N distances are about 0.1 Å longer than

Table 1. Selected bond lengths [Å] and angles [°] for $[Pd_2Ag_2(\mu\text{-}pz)_6]\cdot 3CH_3CN$ (**1**·3 CH_3CN).

Ag1···Pd1	3.4609(3)	Ag2···Pd2	3.4710(3)
Ag1···Pd2	3.4456(3)	Pd1···Pd2	3.4341(3)
Ag2···Pd1	3.4712(3)		
Ag1–N32	2.105(3)	Pd1–N31	2.008(2)
Ag1–N52	2.106(3)	Pd1–N41	2.006(2)
Ag2–N42	2.103(3)	Pd2–N11	2.013(2)
Ag2–N62	2.105(3)	Pd2–N21	2.011(2)
Pd1–N12	2.004(2)	Pd2–N51	2.013(2)
Pd1–N22	2.007(2)	Pd2–N61	2.008(2)
N32-Ag1-N52	174.5(1)	N51-Pd2-N61	91.82(9)
N42-Ag2-N62	167.5(1)	Pd2-N11-N12	121.7(2)
N12-Pd1-N22	89.26(9)	Pd1-N12-N11	120.7(2)
N12-Pd1-N31	179.16(9)	Pd2-N21-N22	121.2(2)
N12-Pd1-N41	89.72(9)	Pd1-N22-N21	120.9(2)
N22-Pd1-N31	89.91(9)	Pd1-N31-N32	120.8(2)
N22-Pd1-N41	178.96(9)	Ag1-N32-N31	120.3(2)
N31-Pd1-N41	91.1(1)	Pd1-N41-N42	119.7(2)
N11-Pd2-N21	89.53(9)	Ag2-N42-N41	122.1(2)
N11-Pd2-N51	179.08(9)	Pd2-N51-N52	120.6(2)
N11-Pd2-N61	89.08(9)	Ag1-N52-N51	120.3(2)
N21-Pd2-N51	89.57(9)	Pd2-N61-N62	119.8(2)
N21-Pd2-N61	178.61(9)	Ag2-N62-N61	121.6(2)

the Pd–N distances as the ionic radius of Ag^{I} is larger than that of Pd^{II}. In the crystals containing no solvent molecule, which were obtained by following method B in Scheme 2, the complex molecule **1** interacts with a neighboring molecule through the Ag atoms (Figure 2). The Ag2···Ag2* distance (2.995(2) Å) is 0.4 Å or more shorter than the intra-

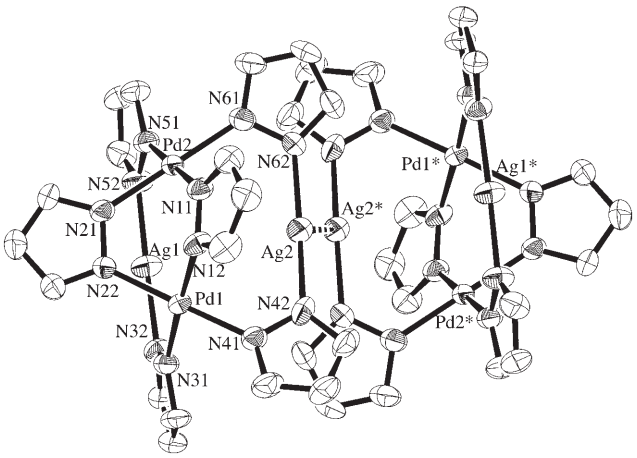

Figure 2. Ag···Ag contact between molecules of **1** related by the center of symmetry.

molecular Pd···Ag and Pd···Pd contacts (Table 2). Because the corresponding bond distances and angles in **1** and **1**·3 CH_3CN are similar, the effect of solvent molecules or intermolecular Ag···Ag contacts on the interatomic distances and angles must be small.

Table 2. Selected bond lengths [Å] and angles [°] for $[Pd_2Ag_2(\mu\text{-}pz)_6]$ (**1**).

Ag1···Pd1	3.460(1)	Ag2···Pd1	3.4209(9)
Ag1···Pd2	3.439(1)	Ag2···Pd2	3.399(1)
Ag2···Ag2*	2.995(2)	Pd1···Pd2	3.4232(8)
Ag1–N32	2.099(7)	Pd1–N31	2.025(8)
Ag1–N52	2.085(7)	Pd1–N41	1.999(7)
Ag2–N42	2.082(9)	Pd2–N11	2.012(8)
Ag2–N62	2.100(8)	Pd2–N21	2.010(7)
Pd1–N12	1.999(8)	Pd2–N51	2.023(8)
Pd1–N22	2.025(7)	Pd2–N61	1.993(8)
N32-Ag1-N52	176.4(3)	N21-Pd2-N61	178.7(3)
Ag2-Ag2-N42	110.6(2)	N51-Pd2-N61	91.0(3)
Ag2-Ag2-N62	79.0(2)	Pd2-N11-N12	121.0(5)
N42-Ag2-N62	170.3(3)	Pd1-N12-N11	120.1(6)
N12-Pd1-N22	90.3(3)	Pd2-N21-N22	121.6(5)
N12-Pd1-N31	176.6(3)	Pd1-N22-N21	119.3(5)
N12-Pd1-N41	87.7(3)	Pd1-N31-N32	122.1(5)
N22-Pd1-N31	91.6(3)	Ag1-N32-N31	119.7(5)
N22-Pd1-N41	177.9(3)	Pd1-N41-N42	119.9(6)
N31-Pd1-N41	90.5(3)	Ag2-N42-N41	120.0(5)
N11-Pd2-N21	90.4(3)	Pd2-N51-N52	120.2(5)
N11-Pd2-N51	179.0(3)	Ag1-N52-N51	120.4(6)
N11-Pd2-N61	88.5(3)	Pd2-N61-N62	120.9(6)
N21-Pd2-N51	90.1(3)	Ag2-N62-N61	118.4(5)

Figure 3 illustrates one of the pair of complex molecules $[Pd_2Au_2(\mu\text{-}pz)_6]$ (**2**) in (**2**)$_2$·3 $CH_3CN\cdot H_2O$, which contains two crystallographically independent pairs of complex mole-

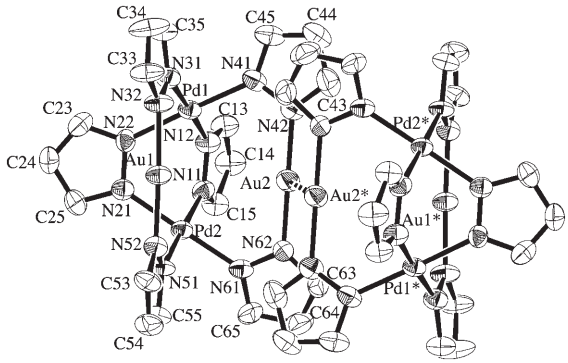

Figure 3. Au···Au contact between molecules of $[Pd_2Au_2(\mu\text{-}pz)_6]$ (**2**) related by the center of symmetry.

cules in the asymmetric unit. There is an intermolecular Au···Au contact within the pair in which the complex molecules are related by a center of symmetry, the Au2···Au2* and Au4···Au4* distances being 3.154(1) and 3.181(1) Å, respectively (Table 3). There is also a weaker Au1···Au3* contact (3.4050(7) Å) between the independent pairs of complex molecules in an asymmetric unit. The Pd···M (M = Au or Ag) and Pd···Pd distances in (**2**)$_2$·3 $CH_3CN\cdot H_2O$ are similar to those in **1** and **1**·3 CH_3CN. The Au–N distances, however, are similar to the Pd···N distances in (**2**)$_2$·3 $CH_3CN\cdot H_2O$. This tendency is different from that in **1** and **1**·3 CH_3CN, in which the Ag–N distances are about 0.1 Å longer than the Pd–N distances.

When 3-*t*Bupz$^-$ was employed as the bridging ligand, the main products were the *HT* and *HH* isomers arising from

Table 3. Selected bond lengths [Å] and angles [°] for $[Pd_2Au_2(\mu\text{-}pz)_6]_2\cdot 3CH_3CN\cdot H_2O$ ($(\mathbf{2})_2\cdot 3CH_3CN\cdot H_2O$).

Au1···Au3*	3.4050(7)	Au3···Pd4	3.396(1)
Au1···Pd1	3.421(1)	Au4···Au4*	3.181(1)
Au1···Pd2	3.444(1)	Au4···Pd3	3.358(1)
Au2···Au2*	3.154(1)	Au4···Pd4	3.434(1)
Au2···Pd1	3.421(1)	Pd1···Pd2	3.363(1)
Au2···Pd2	3.352(1)	Pd3···Pd4	3.362(1)
Au3···Pd3	3.465(1)		
Au1−N32	2.01(1)	Pd2−N11	2.02(1)
Au1−N52	2.01(1)	Pd2−N21	2.00(1)
Au2−N42	2.01(1)	Pd2−N51	2.03(1)
Au2−N62	2.00(1)	Pd2−N61	2.00(1)
Au3−N92	1.98(1)	Pd3−N72	1.99(1)
Au3−N112	1.99(1)	Pd3−N82	2.02(1)
Au4−N102	1.99(1)	Pd3−N91	2.03(1)
Au4−N122	1.99(1)	Pd3−N101	2.00(1)
Pd1−N12	2.00(1)	Pd4−N71	2.01(1)
Pd1−N22	2.00(1)	Pd4−N81	2.01(1)
Pd1−N31	2.00(1)	Pd4−N111	2.01(1)
Pd1−N41	2.01(1)	Pd4−N121	2.01(1)
N32-Au1-N52	176.3(5)	N71-Pd4-N121	91.6(5)
Au2-Au2-N42	93.3(3)	N81-Pd4-N111	90.9(4)
Au2-Au2-N62	93.8(3)	N81-Pd4-N121	176.9(5)
N42-Au2-N62	172.7(5)	N111-Pd4-N121	89.8(5)
N92-Au3-N112	177.3(4)	Pd2-N11-N12	118.5(8)
Au4-Au4-N102	94.8(3)	Pd1-N12-N11	121.2(8)
Au4-Au4-N122	92.5(3)	Pd2-N21-N22	120.6(8)
N102-Au4-N122	172.5(5)	Pd1-N22-N21	119.0(7)
N12-Pd1-N22	87.5(4)	Pd1-N31-N32	122.0(8)
N12-Pd1-N31	177.5(4)	Au1-N32-N31	119.0(8)
N12-Pd1-N41	93.3(4)	Pd1-N41-N42	119.9(8)
N22-Pd1-N31	90.1(4)	Au2-N42-N41	120.5(8)
N22-Pd1-N41	177.7(4)	Pd2-N51-N52	122.0(7)
N31-Pd1-N41	89.1(4)	Au1-N52-N51	120.5(8)
N11-Pd2-N21	88.7(4)	Pd2-N61-N62	119.8(8)
N11-Pd2-N51	177.7(4)	Au2-N62-N61	118.9(8)
N11-Pd2-N61	89.7(4)	Pd4-N71-N72	120.7(8)
N21-Pd2-N51	92.1(4)	Pd3-N72-N71	119.3(9)
N21-Pd2-N61	178.4(4)	Pd4-N81-N82	120.0(8)
N51-Pd2-N61	89.4(4)	Pd3-N82-N81	120.5(8)
N72-Pd3-N82	88.1(4)	Pd3-N91-N92	121.4(8)
N72-Pd3-N91	176.2(5)	Au3-N92-N91	121.5(8)
N72-Pd3-N101	90.1(4)	Pd3-N101-N102	119.1(9)
N82-Pd3-N91	93.4(4)	Au4-N102-N101	118.9(8)
N82-Pd3-N101	178.1(4)	Pd4-N111-N112	120.7(8)
N91-Pd3-N101	88.5(4)	Au3-N112-N111	120.2(8)
N71-Pd4-N81	87.7(4)	Pd4-N121-N122	119.8(9)
N71-Pd4-N111	178.4(5)	Au4-N122-N121	121.5(9)

the different orientation of the substituent groups on the pyrazolate bridges between the two Pd atoms. The X-ray structural analysis disclosed that the product (**4a**) obtained from the reaction of *HT*-$[Pd_2(\mu\text{-}3\text{-}t\text{Bupz})_2(3\text{-}t\text{Bupz})_2(3\text{-}t\text{BupzH})_2]$ with [AuCl(tht)] was the *HT* isomer, in which the bridging nature of the $Pd(\mu\text{-}3\text{-}t\text{Bupz})_2Pd$ moiety has been retained (Figure 4). The complex molecule **4a** has an approximate twofold axis passing through the midpoints of the Pd1···Pd2 and Au1···Au2 contacts. Although the structural parameters of **4a** are not suitable for a detailed comparison owing to their large standard deviations, there may be a tendency, due to the bulkiness of the substituent group, that the Pd−N distances in the Pd···Pd bridges close to the *tert*-butyl group (Pd1−N22 and Pd2−N12) are longer than the average

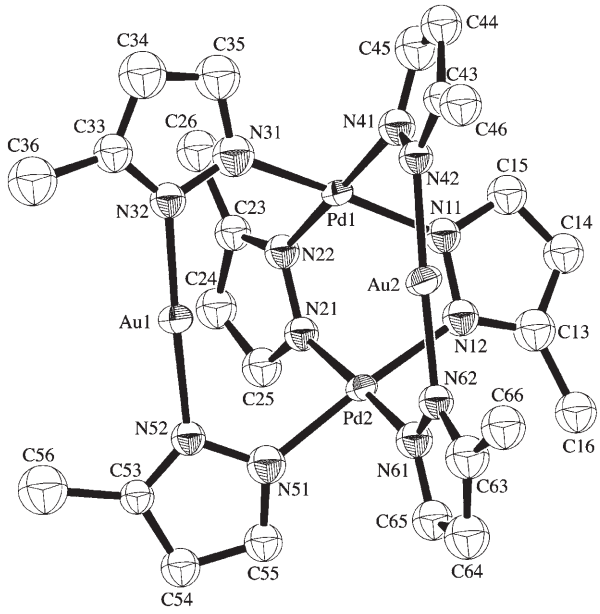

Figure 4. Molecular structure of the head-to-tail isomer of $[Pd_2Au_2(\mu\text{-}3\text{-}t\text{Bupz})_6]$ (**4a**) with the atom numbering scheme (50% probability ellipsoids). Methyl carbon atoms in the *tert*-butyl groups have been omitted for clarity.

Pd−N distances in the Pd···Au bridges, while the Pd−N distances in the Pd···Pd bridges far from the *tert*-butyl group (Pd1−N11 and Pd2−N21) are shorter than the average Pd−N distances in the Pd···Au bridges (Table 4).

Table 4. Selected bond lengths [Å] and angles [°] for *HT*-$[Pd_2Au_2(\mu\text{-}3\text{-}t\text{Bupz})_6]\cdot CH_3CN$ (**4a**·CH_3CN).

Au1···Pd1	3.474(2)	Au2··Pd2	3.457(2)
Au1··Pd2	3.392(2)	Pd1··Pd2	3.229(3)
Au2··Pd1	3.357(2)		
Au1−N32	2.00(2)	Pd1−N31	2.02(3)
Au1−N52	2.04(2)	Pd1−N41	2.04(2)
Au2−N42	2.03(2)	Pd2−N12	2.06(2)
Au2−N62	2.01(2)	Pd2−N21	1.97(2)
Pd1−N11	1.98(2)	Pd2−N51	2.02(2)
Pd1−N22	2.04(2)	Pd2−N61	2.02(2)
N32-Au1-N52	177(1)	N51-Pd2-N61	88.6(9)
N42-Au2-N62	174.6(9)	Pd1-N11-N12	122(2)
N11-Pd1-N22	88.1(8)	Pd2-N12-N11	112(2)
N11-Pd1-N31	173(1)	Pd2-N21-N22	123(1)
N11-Pd1-N41	90.3(9)	Pd1-N22-N21	112(1)
N22-Pd1-N31	95.8(9)	Pd1-N31-N32	129(2)
N22-Pd1-N41	175.0(9)	Au1-N32-N31	115(2)
N31-Pd1-N41	86.4(9)	Pd1-N41-N42	122(2)
N12-Pd2-N21	87.3(9)	Au2-N42-N41	117(2)
N12-Pd2-N51	170.5(9)	Pd2-N51-N52	123(2)
N12-Pd2-N61	96.1(9)	Au1-N52-N51	116(2)
N21-Pd2-N51	88.6(9)	Pd2-N61-N62	126(2)
N21-Pd2-N61	175(1)	Au2-N62-N61	118(2)

The molecular structure of the *HH* isomer **4b**, obtained by isomerization of **4a**, is illustrated in Figure 5. The complex molecule has an idealized mirror plane defined by two Pd atoms and the midpoint of the Au···Au contact, which is

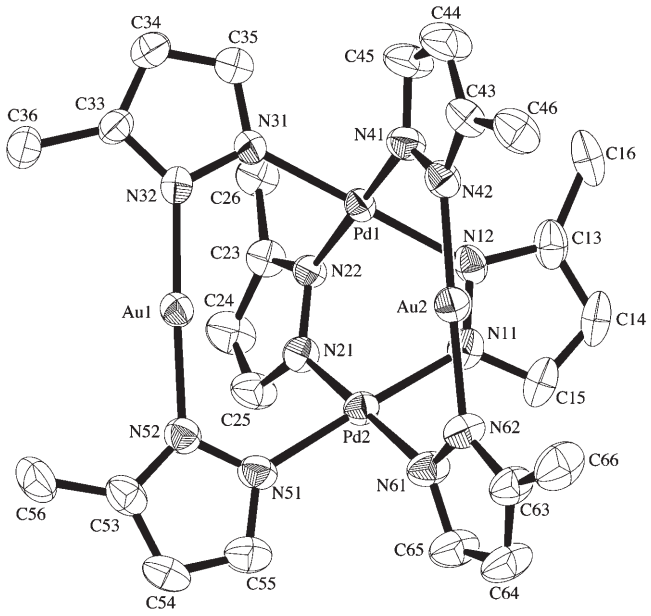

Figure 5. Molecular structure of the head-to-head isomer of $[Pd_2Au_2(\mu\text{-}3\text{-}t\text{Bupz})_6]$ (**4b**) with the atom numbering scheme (50% probability ellipsoids). Methyl carbon atoms in the *tert*-butyl groups have been omitted for clarity.

consistent with the observation of the existence of three inequivalent 3-*t*Bupz ligands by ^{1}H NMR spectroscopy. The structure of **4b** is very similar to that of *HH*-$[Pd_2Ag_2(\mu\text{-}3\text{-}t\text{Bupz})_6]$,[9] although **4b** crystallizes with one molecule of CH_3CN while *HH*-$[Pd_2Ag_2(\mu\text{-}3\text{-}t\text{Bupz})_6]$ crystallizes with two; the crystals **4b**·CH_3CN and *HH*-$[Pd_2Ag_2(\mu\text{-}3\text{-}t\text{Bupz})_6]\cdot 2\,CH_3CN$ are not isomorphous. The average Au–N distance in **4b** (2.023 Å) is 0.09 Å shorter than the average Ag–N distance in *HH*-$[Pd_2Ag_2(\mu\text{-}3\text{-}t\text{Bupz})_6]$ (2.111 Å; Table 5). Similarly to the cases of **4a** and *HH*-$[Pd_2Ag_2(\mu\text{-}3\text{-}t\text{Bupz})_6]$, an elongation of the Pd–N distances in the Pd···Pd bridges close to *tert*-butyl group was observed for **4b** due to the bulkiness of the substituent group; the Pd1–N12 (2.044(6) Å) and Pd1–N22 distances (2.047(5) Å) are about 0.03 Å longer than the average Pd–N distance (2.018 Å) in the Pd···Au bridges.

Table 5. Selected bond lengths [Å] and angles [°] for *HH*-$[Pd_2Au_2(\mu\text{-}3\text{-}t\text{Bupz})_6]\cdot CH_3CN$ (**4b**·CH_3CN).

Au1···Pd1	3.5011(6)	Au2···Pd2	3.3497(5)
Au1···Pd2	3.4123(5)	Pd1···Pd2	3.2676(7)
Au2···Pd1	3.5386(2)		
Au1–N32	2.013(6)	Pd1–N31	2.014(5)
Au1–N52	2.029(6)	Pd1–N41	2.029(6)
Au2–N42	2.014(6)	Pd2–N11	1.997(6)
Au2–N62	2.036(6)	Pd2–N21	1.998(5)
Pd1–N12	2.044(6)	Pd2–N51	2.027(6)
Pd1–N22	2.047(5)	Pd2–N61	2.003(6)
N32-Au1-N52	175.9(2)	N51-Pd2-N61	90.8(3)
N42-Au2-N62	175.6(2)	Pd2-N11-N12	123.3(4)
N12-Pd1-N22	88.0(2)	Pd1-N12-N11	113.4(4)
N12-Pd1-N31	178.3(2)	Pd2-N21-N22	122.8(4)
N12-Pd1-N41	93.1(2)	Pd1-N22-N21	111.8(4)
N22-Pd1-N31	90.5(2)	Pd1-N31-N32	125.7(4)
N22-Pd1-N41	176.7(2)	Au1-N32-N31	118.4(4)
N31-Pd1-N41	88.5(2)	Pd1-N41-N42	126.2(4)
N11-Pd2-N21	89.6(2)	Au2-N42-N41	118.6(4)
N11-Pd2-N51	178.2(2)	Pd2-N51-N52	123.8(4)
N11-Pd2-N61	88.3(2)	Au1-N52-N51	116.9(4)
N21-Pd2-N51	91.1(2)	Pd2-N61-N62	123.8(4)
N21-Pd2-N61	174.3(2)	Au2-N62-N61	115.4(4)

In connection with the mechanism of isomerization of *HH*- and *HT*-$[Pd_2M'_2(\mu\text{-}3\text{-}t\text{Bupz})_6]$ (M′ = Ag, Au), it may be worthwhile to compare the geometry of the pyrazolate bridges between the two Pd atoms. We define the terms "tilt angle" as the angle between the two Pd planes (τ) and the "twist angle" as that of the two Pd planes about the Pd···Pd axis (ω), as shown in Scheme 4. Because two sites of each Pd plane are directly connected by pyrazolate bridges, the Pd···Pd distance and the tilt angle are affected primarily by the M′–N (N–M′–N) distances. They are also affected by the rotation of the Pd planes about the Pd···Pd axis and the elongation of the Pd–N bond close to the *tert*-butyl group, which release the strain of the Pd···Pd bridges. It is reasonable that the Pd···Pd distance in **3b** (3.3801(3) Å) is longer than that in **4b** (3.268(1) Å) and the tilt angle in **3b** (88.9(1)°) is larger than that in **4b** (84.7(3)°) because the Ag–N distances in **3b** are about 0.1 Å longer than the Au–N distances in **4b**. The longer Pd···Pd distance and the larger tilt angle in **4b** than in **4a** are attributable to the smaller twist angle in **4b**. The structural parameters of these three complexes (**4a**, **4b**, and **3b**) may imply that the rotation of the Pd planes about the Pd···Pd axis is more restricted for the *HH* isomer than that for the *HT* isomer due to the steric repulsion between the bulky substituent groups. However, it is difficult to estimate the difference in the degree of molecular strain between *HH* and *HT* isomers because the differences between the structural parameters of the two isomers are small and their number is limited.

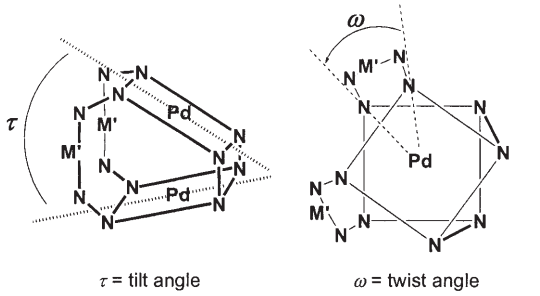

Complex	Pd···Pd distance [Å]	τ [°]	ω [°]	N-M'-N [°]
4a	3.228(3)	79.5(8)	10.0(10)	175.6 (av)
4b	3.268(1)	84.7(3)	6.6(3)	175.8 (av)
3b	3.3801(3)	88.9(1)	3.7(1)	174.21 (av)

Scheme 4. Technical terms used in the structural discussion.

Isomerization: Two geometrical isomers (*HT* (**4a**) and *HH* (**4b**)) arising from the relative orientation of the substituent

groups on the pyrazolate bridges between the two Pd atoms have been isolated as major products for $[Pd_2Au_2(\mu\text{-}3\text{-}t\text{Bupz})_6]$ out of several possible isomers even though the precursor *HT*-$[Pd_2(\mu\text{-}3\text{-}t\text{Bupz})_2(3\text{-}t\text{Bupz})_2(3\text{-}t\text{BupzH})_2]$ does not isomerize, even at elevated temperatures. It is also possible to isolate a similar pair of isomers for $[Pd_2Ag_2(\mu\text{-}3\text{-}t\text{Bupz})_6]$ (*HT* (**3a**) and *HH* (**3b**)). Because **3b** and **4a** are easier to isolate than **3a** and **4b**, isomerization reactions of the former complexes were followed by ^{1}H NMR spectroscopy. The spectral variations due to the isomerization of **3b** in $CDCl_3$ at 40 °C and those of **4a** in C_6D_6 at 50 °C are shown in Figures 6 and 7, respectively. No species other than **3a** and **4b** appear during the isomerization of **3b** and **4a**.

As the concentrations of **3b** and **3a** are proportional to the relative values of the integrated intensities of their corresponding proton resonances, those of the H_5 resonances at specific time intervals are plotted against the time in Figure 8. Similar to the isomerization of *HH*-$[Pt_2(en)_2(\alpha\text{-pyridonate})_2](NO_3)_2$,[15] the time-dependence of the disappearance of **3b** and the appearance of **3a** (Figure 8) is best fitted to the integrated form of a rate law [Eq. (1)] that describes a first-order approach to equilibrium [Eq. (2)]. Typical fits of the time-dependent change in the relative values of the integrated intensities of **3b** and **3a** to Equations (3) and (4) are given in the upper and lower traces, respectively, in Figure 8. We define the rate of isomerization from the *HT* to the *HH* isomer and that from the *HH* to the *HT* isomer as k_1 and k_2, respectively.

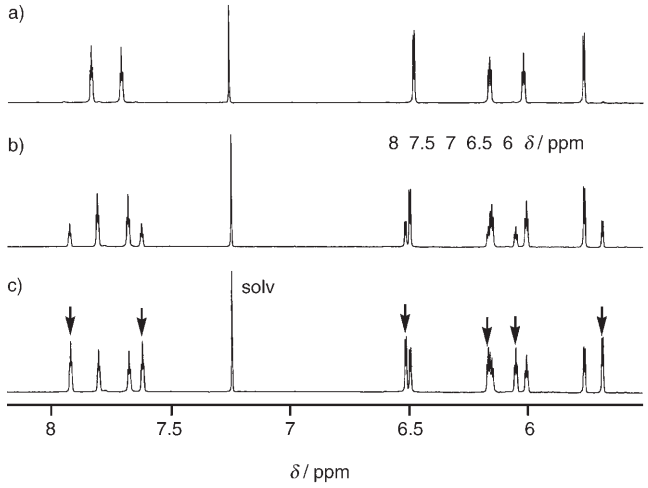

Figure 6. ^{1}H NMR spectral variations due to the isomerization of *HH*-$[Pd_2Ag_2(\mu\text{-}3\text{-}t\text{Bupz})_6]$ (**3b**) (initial concentration: 15.5 mM) in $CDCl_3$: a) 20 °C, before isomerization; b) 40 °C for 110 min; c) 40 °C for 780 min. The arrows show new signals arising from the isomerization.

$$-\mathrm{d}[\mathbf{3b}]/\mathrm{d}t = \mathrm{d}[\mathbf{3a}]/\mathrm{d}t = k_2[\mathbf{3b}] - k_1[\mathbf{3a}] \quad (1)$$

$$\mathbf{3b} \underset{k_1}{\overset{k_2}{\rightleftharpoons}} \mathbf{3a} \quad (2)$$

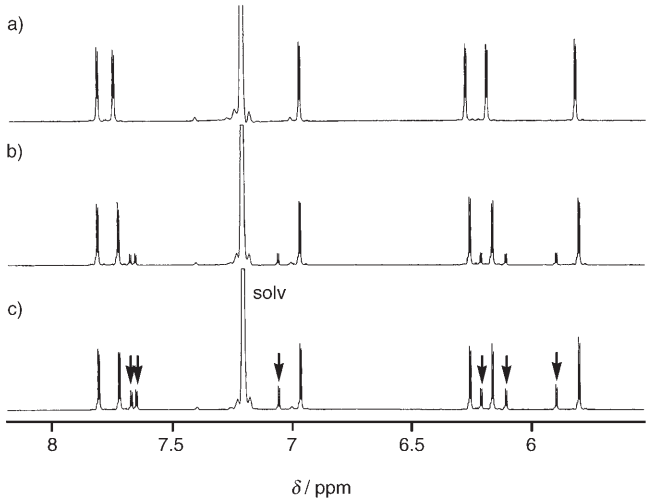

Figure 7. ^{1}H NMR spectral variations due to the isomerization of *HT*-$[Pd_2Au_2(\mu\text{-}3\text{-}t\text{Bupz})_6]$ (**4a**) (initial concentration: 14.6 mM) in C_6D_6: a) 20 °C, before isomerization; b) 50 °C for 240 min; c) 50 °C for 900 min. The arrows show new signals arising from the isomerization.

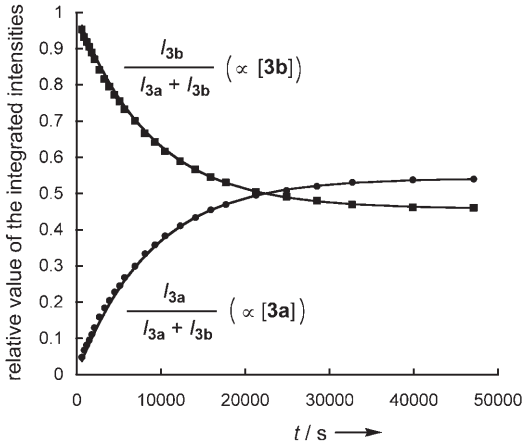

Figure 8. The variation with time of the relative value of the integrated intensities of H_5 in **3a** ($\delta = 7.94$ ppm) and **3b** ($\delta = 7.82$ ppm), which are proportional to the concentration of **3a** and **3b**, in $CDCl_3$ at 40 °C. The solid lines are the calculated appearance of **3a**, $x_t = x_e[1-\exp(-k_{obs}t)]$, and disappearance of **3b**, $x_t = x_e + (x_0 - x_e)[\exp(-k_{obs}t)]$, from a least-squares fit to Equation (4), where $k_{obs} = 1.143 \times 10^{-4}\ s^{-1}$.

$$[\mathbf{3b}]_t = [\mathbf{3b}]_{eq} + ([\mathbf{3b}]_0 - [\mathbf{3b}]_{eq})[\exp(-(k_1 + k_2)t)] \quad (3)$$

$$[\mathbf{3a}]_t = [\mathbf{3a}]_{eq}[1 - \exp(-(k_1 + k_2)t)] \quad (4)$$

The rate and equilibrium constants as functions of temperature are summarized in Table 6. An Eyring plot of the temperature-dependence of the rate constant, $\ln(k/T)$ versus $1/T$, revealed the activation parameters for the *HH*⇄*HT* isomerization of $[Pd_2Ag_2(\mu\text{-}3\text{-}t\text{Bupz})_6]$ to be $\Delta H^{\neq} = 100(1)\ kJ\,mol^{-1}$ and $\Delta S^{\neq} = 0(3)\ J\,mol^{-1}\,K^{-1}$.

The relative values of the integrated intensities of the H_4 resonances at specific time intervals are plotted against the time for **4a** and **4b** in C_6D_6 at 50 °C in Figure 9. Similarly to the isomerization of **3b**, the time-dependence of the disap-

Table 6. Rate and equilibrium data for the *HH* (**3b**) ⇄ *HT* (**3a**) isomerization of $[Pd_2Ag_2(\mu\text{-}3\text{-}t\text{Bupz})_6]$.

Run	Solvent	Init. conc. of **3b** [mM]	T [°C]	K_{eq}[a]	$10^5\,k_{obs}$ [s^{-1}]	$10^5\,k_1$[b] [s^{-1}]	$10^5\,k_2$[b] [s^{-1}]
1	$CDCl_3$	15.5	40	1.19	11.43(9)[c]	5.23	6.20
2	$CDCl_3$	15.4	45	1.22	21.2(2)[c]	9.5	11.7
3	$CDCl_3$	15.4	50	1.24	38.6(5)[c]	17.3	21.3
4	$CDCl_3$	15.7	55	1.27	69.9(5)[c]	30.8	39.1
5	C_6D_6	15.5	50	1.35	32.4(3)[d]	13.8	18.6

[a] After each kinetics run the sample was incubated for approximately 20 half-lives at the specified temperature. Equilibrium constants were calculated from the relative value of the integrated intensities. [b] k_1 and k_2 were calculated from the equations $k_{obs}=k_1+k_2$ and $K_{eq}=k_2/k_1$. [c] k_{obs} for disappearance of the *HH* isomer resonance at $\delta=7.82$ ppm and appearance of the *HT* isomer resonance at $\delta=7.94$ ppm were calculated from Equations (3) and (4). [d] k_{obs} for disappearance of the *HH* isomer resonance at $\delta=6.27$ ppm and appearance of the *HT* isomer resonance at $\delta=6.36$ ppm were calculated from Equations (3) and (4).

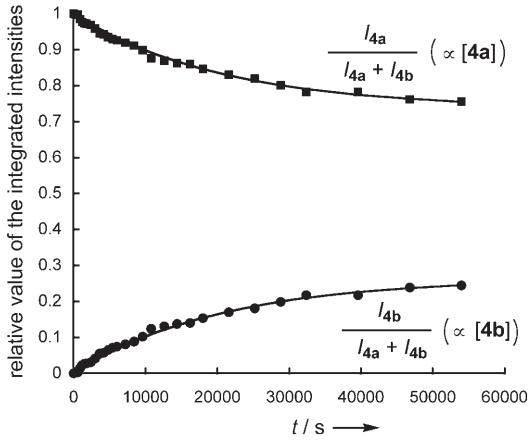

Figure 9. The variation with time of the relative value of the integrated intensities of H_4 in **4a** ($\delta=5.81$ ppm) and **4b** ($\delta=5.92$ ppm), which are proportional to the concentration of **4a** and **4b**, in C_6D_6 at 50 °C. The solid lines are the calculated appearance of **4b**, $x_t=x_e[1-\exp(-k_{obs}t)]$, and disappearance of **4a**, $x_t=x_e+(x_0-x_e)[\exp(-k_{obs}t)]$ from a least-squares fit to Equation (8), where $k_{obs}=4.78\times10^{-5}\,s^{-1}$.

pearance of **4a** and the appearance of **4b** is also best fit to the integrated form of a rate law [Eq. (5)] that describes a first-order approach to equilibrium [Eq. (6)]. Typical fits of the time-dependent change in the relative values of the integrated intensities of **4a** and **4b** to Equations (7) and (8) are given in the upper and lower traces, respectively, in Figure 9.

$$-\mathrm{d}[\mathbf{4a}]/\mathrm{d}t = \mathrm{d}[\mathbf{4b}]/\mathrm{d}t = k_1[\mathbf{4a}]-k_2[\mathbf{4b}] \quad (5)$$

$$\mathbf{4a} \underset{k_2}{\overset{k_1}{\rightleftharpoons}} \mathbf{4b} \quad (6)$$

$$[\mathbf{4a}]_t = [\mathbf{4a}]_{eq} + ([\mathbf{4a}]_0-[\mathbf{4a}]_{eq})[\exp(-(k_1+k_2)t)] \quad (7)$$

$$[\mathbf{4b}]_t = [\mathbf{4b}]_{eq}[1-\exp(-(k_1+k_2)t)] \quad (8)$$

The rate and equilibrium constants as functions of temperature are summarized in Table 7. The kinetic measurements made with **4b** in C_6D_6 at 60 °C (run 9, Figure 10) reveal that the k_1 and k_2 values are almost identical to those obtained with **4a** under the same conditions, thus showing the validity of the assumption of equilibrium in Equation (6) and therefore that in Equation (2). The rate of isomerization is scarcely affected by the concentration of the complex (runs 7 and 8) or by the presence of neutral bridging ligands (run 10). An Eyring plot of the temperature-dependence of the rate constant, $\ln(k/T)$ versus $1/T$, revealed the activation parameters for the *HH*⇄*HT* isomerization of $[Pd_2Au_2(\mu\text{-}3\text{-}t\text{Bupz})_6]$ to be $\Delta H^{\neq}=112(5)\,kJ\,mol^{-1}$ and $\Delta S^{\neq}=20(17)\,J\,mol^{-1}\,K^{-1}$.

Table 7. Rate and equilibrium data for the *HT* (**4a**) ⇄ *HH* (**4b**) isomerization of $[Pd_2Au_2(\mu\text{-}3\text{-}t\text{Bupz})_6]$

Run	Solvent	Init. conc. of **4a** [mM]	T [°C]	K_{eq}[a]	$10^5\,k_{obs}$ [s^{-1}]	$10^5\,k_1$[b] [s^{-1}]	$10^5\,k_2$[b] [s^{-1}]
1	C_6D_6	14.6	50	0.36	4.78(8)[c]	1.26	3.52
2	C_6D_6	14.5	55	0.36	10.4(2)[c]	2.8	7.6
3	C_6D_6	15.2	60	0.36	17.7(3)[c]	4.7	13.0
4	C_6D_6	15.1	65	0.36	33.0(7)[c]	8.7	24.3
5	$CDCl_3$	11.5	50	0.36	7.2(1)[d]	1.9	5.3
6	$CDCl_3$	13.1	55	0.36	10.3(3)[d]	2.7	7.6
7	C_6D_6	4.0	60	0.36	15.6(4)[c]	4.1	11.5
8	C_6D_6	60.0	60	0.36	16.04(9)[c]	4.26	11.78
9	C_6D_6	6.6[e]	60	0.36	17.3(2)[f]	4.6	12.7
10	C_6D_6	14.5	60	0.36	17.9(3)[c, g]	4.7[g]	13.2[g]

[a] After each kinetics run the sample was incubated for approximately 20 half-lives at the specified temperature. Equilibrium constants were calculated from the relative value of the integrated intensities. [b] k_1 and k_2 were calculated from the equations $k_{obs}=k_1+k_2$ and $K_{eq}=k_1/k_2$. [c] k_{obs} for disappearance of the *HT* isomer resonance at $\delta=5.81$ ppm and appearance of the *HH* isomer resonance at $\delta=5.92$ ppm were calculated from Equations (7) and (8). [d] k_{obs} for disappearance of the *HT* isomer resonance at $\delta=5.68$ ppm and appearance of the *HH* isomer resonance at $\delta=5.75$ ppm were calculated from Equations (7) and (8). [e] Initial concentration of **4b** (mM). [f] k_{obs} for appearance of the *HT* isomer resonance at $\delta=5.81$ ppm and disappearance of the *HH* isomer resonance at $\delta=5.92$ ppm were calculated from Equations (7′) and (8′). {$-\mathrm{d}[\mathbf{4b}]/\mathrm{d}t=\mathrm{d}[\mathbf{4a}]/\mathrm{d}t=k_2[\mathbf{4b}]-k_1[\mathbf{4a}]$ (5′), $\mathbf{4b} \underset{k_1}{\overset{k_2}{\rightleftharpoons}} \mathbf{4a}$ (6′), $[\mathbf{4b}]_t=[\mathbf{4b}]_{eq}+([\mathbf{4b}]_0-[\mathbf{4b}]_{eq})[\exp(-(k_1+k_2)t]$ (7′), $[\mathbf{4a}]_t=[\mathbf{4a}]_{eq}[1-\exp(-(k_1+k_2)t)]$ (8′)}. [g] Rate in the presence of 2.1 equivalents of 3-*t*BupzH.

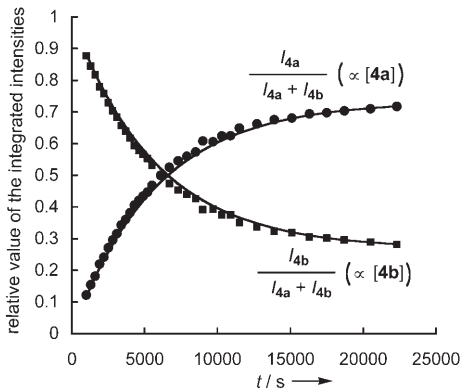

Figure 10. The variation with time of the relative value of the integrated intensities of H_4 in **4a** ($\delta = 5.81$ ppm) and **4b** ($\delta = 5.92$ ppm), which are proportional to the concentration of **4a** and **4b**, in C_6D_6 at 60 °C. The solid lines are the calculated appearance of **4a**, $x_t = x_e[1-\exp(-k_{obs}t)]$, and disappearance of **4b**, $x_t = x_e + (x_0 - x_e)[\exp(-k_{obs}t)]$ from a least-squares fit to Equation (8′) (see footnote to Table 7) where $k_{obs} = 1.73 \times 10^{-4}\ s^{-1}$.

A comparison of Tables 6 and 7 revealed that the concentration of the *HT* isomer is higher than that of the *HH* isomer at equilibrium for both $[Pd_2Ag_2(\mu\text{-}3\text{-}t\text{Bupz})_6]$ and $[Pd_2Au_2(\mu\text{-}3\text{-}t\text{Bupz})_6]$. The rate of isomerization from **3a** to **3b** is about 10 times faster than that of **4a** to **4b**, while that of **3b** to **3a** is about five times faster than that of **4b** to **4a**. It is very interesting to note that the rate of isomerization is affected by the nature of the heterometal ions (Ag^I and Au^I), although there is no apparent bonding interaction among these ions and the bridging ligands that participate in the isomerization reaction. The reason why the isomerization of $[Pd_2Ag_2(\mu\text{-}3\text{-}t\text{Bupz})_6]$, which contains more-labile Ag^I ions, is faster than that of $[Pd_2Au_2(\mu\text{-}3\text{-}t\text{Bupz})_6]$ is unclear at this stage.[24] It is also difficult to explain the difference between the equilibrium constants, K_{eq}, in $[Pd_2Ag_2(\mu\text{-}3\text{-}t\text{Bupz})_6]$ and $[Pd_2Au_2(\mu\text{-}3\text{-}t\text{Bupz})_6]$.

The mechanism of the *HH*⇄*HT* isomerization in $[Pt_2(en)_2(\alpha\text{-pyridonate})_2](NO_3)_2$ is considered to be dissociative due to several reasons: i) the large enthalpy ($\Delta H^{\neq} = 114(5)\ kJ\,mol^{-1}$) and the small positive entropy ($\Delta S^{\neq} = 40(10)\ J\,mol^{-1}\,K^{-1}$), ii) an addition of a better nucleophile to the solution does not affect the rate of isomerization, and iii) the rate of isomerization is accelerated in sterically more hindered $[Pt_2(en)_2(\alpha\text{-pyridonate})_2](NO_3)_2$ than sterically less hindered $[Pt_2(NH_3)_4(\alpha\text{-pyridonate})_2](NO_3)_2$.[15] In the *HH*⇄*HT* isomerization of $[Pd_2Ag_2(\mu\text{-}3\text{-}t\text{Bupz})_6]$ and $[Pd_2Au_2(\mu\text{-}3\text{-}t\text{Bupz})_6]$, a large enthalpy and small positive entropy were also observed and the rate of isomerization was little affected by the nature of the solvent ($CDCl_3$ or C_6D_6). The presence of neutral bridging ligands also does not affect the rate of isomerization, which strongly suggests that the isomerization is an intramolecular exchange reaction. It is thus reasonable to consider that the mechanism of the *HH*⇄*HT* isomerization in $[Pd_2Ag_2(\mu\text{-}3\text{-}t\text{Bupz})_6]$ and $[Pd_2Au_2(\mu\text{-}3\text{-}t\text{Bupz})_6]$ is dissociative.[24]

Conclusion

The heteropolynuclear complexes $[Pd_2M'_2(L)_6]$ ($M'^I = Ag^I$, Au^I; L = pz, 3-*t*Bupz) have been synthesized and structurally characterized. An intermolecular Ag···Ag or Au···Au contact between adjacent complex molecules is found in some crystal structures of $[Pd_2M'_2(pz)_6]$. When 3-*tert*-butylpyrazolate is employed as a bridging ligand, two linkage isomers (*HT* and *HH*) arise from the difference in orientation of the substituent groups on the pyrazolate bridges between the two Pd atoms; they are in equilibrium in solution. This isomerization occurs only at the Pd···Pd bridges—the ligands at the Pd···Ag and Pd···Au bridges apparently do not participate in the isomerization. However, the rate of isomerization is affected by the nature of the heterometal ions (Ag^I and Au^I) present.

Experimental Section

Materials: $[PdCl_2(CH_3CN)_2]$,[17] $[Pd(pzH)_4]Cl_2$,[9] [AuCl(tht)] (tht = tetrahydrothiophene),[18] 3-*tert*-butylpyrazole (3-*t*BupzH),[19] and *HT*-$[Pd_2(\mu\text{-}3\text{-}t\text{Bupz})_2(3\text{-}t\text{Bupz})_2(3\text{-}t\text{BupzH})_2]$[9] were prepared by literature methods. All other commercially available reagents were used as purchased.

Preparation of complexes: $[Pd_2Ag_2(\mu\text{-pz})_6]$ (1): Method A: An acetonitrile solution (10 mL) of $AgPF_6$ (281 mg, 1.11 mmol) was added to a solution of $[Pd(pzH)_4]Cl_2$ (136 mg, 0.30 mmol) in acetonitrile (40 mL) and the resulting solution was stirred for 1 h at 20 °C. The AgCl formed was then filtered off. A solution of Et_3N (156 mg, 1.54 mmol) in acetonitrile (30 mL) was added to the filtrate and the solution was stirred for 2 h at 20 °C. After filtration, the filtrate was concentrated under air. The colorless crystals formed, which contain solvent of crystallization, were collected and washed with acetonitrile. The mother liquid was further concentrated to dryness. The residue was washed with water and diethyl ether to afford a colorless powder. The crystals and powder were then dried in vacuo. Yield: 77 mg (62 %). Elemental analysis calcd (%) for $C_{18}H_{18}Ag_2N_{12}Pd_2$: C 26.02, H 2.18, N 20.23; found: C 26.07, H 1.91, N 20.35; ^{1}H NMR (300 MHz, $CDCl_3$, 25 °C, TMS): $\delta = 5.93$ (t, 2H; H_4), 6.29 (t, 4H; H_4), 6.90 (d, 4H; H_3 and H_5), 7.36 (d, 4H; H_3 or H_5), 7.85 ppm (d, 4H, H_3 or H_5).

Method B: A solution of $AgPF_6$ (461 mg, 1.82 mmol) in acetonitrile (10 mL) was added to a suspension of $[PdCl_2(CH_3CN)_2]$ (105 mg, 0.41 mmol) in acetonitrile (30 mL). The suspension was stirred for 1 h at 20 °C and the resulting AgCl was then filtered off. A solution of Et_3N (193 mg, 1.91 mmol) and pzH (110 mg, 1.61 mmol) in acetonitrile (10 mL) was added to the filtrate, and the solution was stirred for 2 h at 20 °C. After filtration, the filtrate was concentrated under air. The colorless crystals with no solvent of crystallization were collected, washed with acetonitrile, and dried in vacuo. Yield: 34 mg (20 %).

$[Pd_2Au_2(\mu\text{-pz})_6]$ (2): A solution containing $[Pd(pzH)_4]Cl_2$ (98 mg, 0.22 mmol), [AuCl(tht)] (134 mg, 0.42 mmol), and Et_3N (127 mg, 1.25 mmol) in acetonitrile (40 mL) was stirred for 1 h at 20 °C. After filtration, the filtrate was concentrated under air. The colorless crystals were collected, washed with acetonitrile, and dried in vacuo. Yield: 45 mg (41 %). Elemental analysis calcd (%) for $C_{18}H_{18}Au_2N_{12}Pd_2$: C 21.42, H 1.80, N 16.65; found: C 21.46, H 1.66, N 16.65; ^{1}H NMR (300 MHz, $CDCl_3$, 25 °C, TMS): $\delta = 5.98$ (t, 2H; H_4), 6.29 (t, 4H; H_4), 7.02 (d, 4H; H_3 and H_5), 7.33 (d, 4H; H_3 or H_5), 7.80 ppm (d, 4H; H_3 or H_5).

***HT*-$[Pd_2Ag_2(\mu\text{-}3\text{-}t\text{Bupz})_6]$ (3a)**: Et_3N (94 mg, 0.93 mmol) and a solution of $AgPF_6$ (79 mg, 0.31 mmol) in acetonitrile (5 mL) were added to a suspension of *HT*-$[Pd_2(\mu\text{-}3\text{-}t\text{Bupz})_2(3\text{-}t\text{Bupz})_2(3\text{-}t\text{BupzH})_2]$ (139 mg, 0.15 mmol) in acetonitrile (50 mL), and the suspension was stirred for 30 min at 25 °C to give a clear solution. After filtration, the filtrate was

concentrated under air. The crystals, which contained a small amount of *HH* isomer (**3b**), were collected, washed with acetonitrile, and dried in air. Total yield: 101 mg (59%). An attempt to isolate pure **3a** was unsuccessful because isomerization occurs in solution even at room temperature.

***HT*-[Pd_2Au_2(μ-3-*t*Bupz)$_6$] (4a)**: [AuCl(tht)] (66 mg, 0.21 mmol) and a solution of Et_3N (109 mg, 1.08 mmol) acetonitrile (5 mL) were added to a suspension of *HT*-[Pd_2(μ-3-*t*Bupz)$_2$(3-*t*Bupz)$_2$(3-*t*BupzH)$_2$] (98 mg, 0.10 mmol) in acetonitrile (15 mL), and the suspension was stirred for 1 h at 25 °C to give a clear solution. After filtration, the filtrate was concentrated under air. The crystals were collected, washed with acetonitrile, and dried in vacuo. Yield: 101 mg (75%). Elemental analysis calcd (%) for $C_{42}H_{66}Au_2N_{12}Pd_2$: C 37.48, H 4.94, N 12.49; found: C 37.93, H 4.75, N 12.74; ^{1}H NMR (400 MHz, [D_6]benzene, 25 °C; $\delta_{C_6H_6}$ = 7.20 ppm): δ = 1.38 (s, 18H; *t*Bu), 1.45 (s, 18H; *t*Bu), 1.49 (s, 18H; *t*Bu), 5.81 (d, 2H; H_4), 6.18 (d, 2H; H_4), 6.27 (d, 2H; H_4), 6.96 (d, 2H; H_5), 7.73 (d, 2H; H_5), 7.80 ppm (d, 2H; H_5).

***HH*-[Pd_2Au_2(μ-3-*t*Bupz)$_6$] (4b)**: A solution of **4a** (51 mg, 0.038 mmol) in benzene (2 mL) was heated for 2 h at 70 °C. The solution was then loaded onto a preparative TLC plate. The solvent was allowed to evaporate, and product separation was achieved with hexane/CH_2Cl_2 (1:1) as eluent. The minor band was extracted with CH_2Cl_2/CH_3OH (10:1) (3× 30 mL), and the mixture was filtered through Celite. The filtrate was evaporated to dryness, and the residue was dried in vacuo. Crystals suitable for X-ray structural analysis were obtained by recrystallization from CH_3CN. Yield: 6 mg (12%). ^{1}H NMR (400 MHz, [D_6]benzene, 25 °C; $\delta_{C_6H_6}$ = 7.20 ppm): δ = 1.38 (s, 18H; *t*Bu), 1.45 (s, 18H; *t*Bu), 1.49 (s, 18H; *t*Bu), 5.92 (d, 2H; H_4), 6.12 (d, 2H; H_4), 6.22 (d, 2H; H_4), 7.07 (d, 2H; H_5), 7.64 (d, 2H; H_5), 7.66 ppm (d, 2H; H_5).

Kinetic measurements: Because pure samples of the *HH* isomer of [Pd_2Ag_2(μ-3-*t*Bupz)$_6$] (**3b**) and the *HT* isomer of [Pd_2Au_2(μ-3-*t*Bupz)$_6$] (**4a**) are more easily obtained than **3a** and **4b**, the kinetic experiments were mainly carried out with **3b** in $CDCl_3$ and **4a** in C_6D_6. To confirm that the equilibrium condition can be assumed in the rate law, the kinetic experiments were also carried out for **4b** at 60 °C. Before the sample solution was placed into the NMR cell compartment, the desired temperature was achieved. ^{1}H NMR spectra were recorded at a specific time interval (10–30 min, depending on the rate of reaction). No sign of decomposition other than isomerization was observed for **3b** and **4a** during the kinetic runs on the basis of their ^{1}H NMR spectra. The intensity changes of the H_5 resonances of the pyrazolate ligands (δ = 7.94 (**3a**), 7.82 ppm (**3b**)) were followed for [Pd_2Ag_2(μ-3-*t*Bupz)$_6$] in $CDCl_3$, while those of the H_4 resonances (δ = 5.81 ppm (**4a**), 5.92 ppm (**4b**)) were followed for [Pd_2Au_2(μ-3-*t*Bupz)$_6$] in C_6D_6. The integrated peak areas at given times were fit to rate equations by using a nonlinear least-squares program and unit weights.

Equilibrium measurements: After each kinetic run samples were incubated for approximately 20 half-lives at the specified temperature, following which time a spectrum of the system at equilibrium was measured. Equilibrium constants were calculated from the integrated peak areas.

X-ray structural determinations: Crystals suitable for X-ray structural analysis were obtained directly from the reaction mixture. The crystal of **1** was mounted on a glass fiber, while the crystals of **1**·3 CH_3CN, (**2**)$_2$·3 CH_3CN·H_2O, **4a**·CH_3CN, and **4b**·CH_3CN were sealed in thin-walled glass capillaries. Intensity data were collected on a Quantum CCD area detector coupled with a Rigaku AFC7S diffractometer equipped with a graphite-monochromated $Mo_{K\alpha}$ radiation source (λ = 0.71069 Å) at 295–297 K. Final cell parameters were obtained from a least-squares analysis of reflections with $I > 10\sigma(I)$. The data were corrected for Lorentz and polarization effects. An empirical absorption correction was also applied.[20]

The crystal structures of **1**·3 CH_3CN and (**2**)$_2$·3 CH_3CN·H_2O were solved by direct methods (SIR92).[21] Those of **1**, **4a**·CH_3CN, and **4b**·CH_3CN were solved by the heavy-atom method with DIRDIF.[22] The positional and thermal parameters of non-H atoms were refined anisotropically by the full-matrix least-squares method, except for **4a**·CH_3CN, whose Au and Pd atoms were refined anisotropically and N and C atoms isotropically by the full-matrix least-squares method. The minimized function was $\Sigma w(F_o^2 - F_c^2)^2$, where $w^{-1} = \sigma^2(F_o^2) + (p(Max(F_o^2, 0) + 2F_c^2)/3)^2$ (p = 0.05 for **1** and **4a**·CH_3CN, 0.053 for **1**·3 CH_3CN, 0.18 for (**2**)$_2$·3 CH_3CN·H_2O, and 0.10 for **4b**·CH_3CN). Hydrogen atoms were included at calculated positions with fixed displacement parameters (1.2-times the displacement

Table 8. Crystallographic data for [Pd_2Ag_2(μ-pz)$_6$]·3 CH_3CN (**1**·3 CH_3CN), [Pd_2Ag_2(μ-pz)$_6$] (**1**), [Pd_2Au_2(μ-pz)$_6$]$_2$·3 CH_3CN·H_2O ((**2**)$_2$·3 CH_3CN·H_2O), *HT*-[Pd_2Au_2(μ-3-*t*Bupz)$_6$]·CH_3CN (**4a**·CH_3CN), and *HH*-[Pd_2Au_2(μ-3-*t*Bupz)$_6$]·CH_3CN (**4b**·CH_3CN).

	1·3 CH_3CN	**1**	(**2**)$_2$·3 CH_3CN·H_2O	**4a**·CH_3CN	**4b**·CH_3CN
formula	$C_{24}H_{27}Ag_2N_{15}Pd_2$	$C_{18}H_{18}Ag_2N_{12}Pd_2$	$C_{42}H_{47}Au_4N_{27}OPd_4$	$C_{44}H_{69}Au_2N_{13}Pd_2$	$C_{44}H_{69}Au_2N_{13}Pd_2$
Fw	954.11	830.96	2159.48	1386.85	1386.85
T [K]	296	295	296	297	296
λ [Å]	0.71069	0.71069	0.71069	0.71069	0.71069
crystal systems	triclinic	triclinic	triclinic	monoclinic	triclinic
space group	$P\bar{1}$ (no. 2)	$P\bar{1}$ (no. 2)	$P\bar{1}$ (no. 2)	$P2_1/a$ (no. 14)	$P\bar{1}$ (no. 2)
a [Å]	9.0173(3)	9.564(3)	13.843(1)	10.847(3)	12.935(1)
b [Å]	9.8703(6)	11.451(7)	15.019(3)	45.792(2)	13.833(2)
c [Å]	19.056(1)	11.763(5)	16.083(3)	11.322(3)	15.991(1)
α [°]	75.648(1)	66.576(4)	70.239(1)	90	82.672(3)
β [°]	86.6057(9)	82.541(8)	88.106(2)	111.165(1)	73.736(1)
γ [°]	77.3296(6)	87.38(2)	69.603(5)	90	69.736(1)
V [Å^3]	1603.0(1)	1172.1(9)	2935.9(9)	5244(1)	2575.3(5)
Z	2	2	2	4	2
ρ_{calcd} [g cm^{-3}]	1.977	2.354	2.443	1.756	1.788
crystal size [mm]	0.80×0.35×0.15	0.60×0.40×0.15	0.30×0.20×0.06	0.60×0.40×0.30	0.35×0.20×0.20
$2\theta_{max}$ [°]	55.0	55.56	55.04	55.14	55.04
μ($Mo_{K\alpha}$) [mm^{-1}]	2.347	3.186	11.243	6.315	6.429
rflns collected	13711	9450	25294	9683	22092
no. of unique rflns	6784 (R_{int} = 0.016)	4927 (R_{int} = 0.056)	12503 (R_{int} = 0.041)	5819 (R_{int} = 0.053)	10873 (R_{int} = 0.024)
data/restraints/params.	6780/0/388	4178/0/307	12503/0/703	5063/0/265	10873/0/550
final R indices[a]	$R1$ = 0.027 [$I > 2\sigma(I)$]	$R1$ = 0.067 [$I > 3\sigma(I)$]	$R1$ = 0.068 [$I > 2\sigma(I)$]	$R1$ = 0.088 [$I > 3\sigma(I)$]	$R1$ = 0.037 [$I > 2\sigma(I)$]
R indices[b,c]	R = 0.048,[d] R_w = 0.074[d]	R = 0.121, R_w = 0.191	R = 0.144,[d] R_w = 0.202[d]	R = 0.125, R_w = 0.297	R = 0.065,[d] R_w = 0.133[d]
goodness-of-fit on F^2	0.98	2.70	0.87	4.34	1.02
largest diff. peak/hole [e Å^{-3}]	0.75/−0.99	2.79/−2.24	4.03/−4.11	1.41/−2.24	1.93/−2.24

[a] $R1 = \Sigma||F_o| - |F_c||/\Sigma|F_o|$. [b] $R = \Sigma(F_o^2 - F_c^2)/\Sigma F_o^2$. [c] $R_w = [\Sigma\{\omega(F_o^2 - F_c^2)^2\}/\Sigma\{\omega(F_o^2)^2\}]^{1/2}$. [d] All data.

parameters of the host atom). In the final cycle of the refinement, parameter shifts were less than $0.1\,\sigma$. No correction was made for secondary extinction.

All calculations were performed by using teXsan.[23] Further crystallographic data are given in Table 8. Selected bond distances and angles are listed in Tables 1, 2, 3, 4, and 5.

CCDC-281777, CCDC-281778, CCDC-281779, CCDC-281780, and CCDC-281781 contain the supplementary crystallographic data for this paper. These data can be obtained free of charge from The Cambridge Crystallographic Data Centre via www.ccdc.cam.ac.uk/data_request/cif.

Acknowledgments

This work was supported by a Grant-in-Aid for Scientific Research (nos. 17550062 and 16033101). The authors are grateful to Prof. Masaaki Abe at Kyushu University and Prof. Yoichi Sasaki at Hokkaido University for valuable discussions.

[1] a) S. Trofimenko, *Chem. Rev.* **1972**, *72*, 497–509; b) S. Trofimenko, *Prog. Inorg. Chem.* **1986**, *34*, 115–210; c) A. P. Sadimenko, S. S. Basson, *Coord. Chem. Rev.* **1996**, *147*, 247–297; d) G. La Monica, G. A. Ardizzoia, *Prog. Inorg. Chem.* **1997**, *46*, 151–238; e) A. P. Sadimenko, *Adv. Heterocycl. Chem.* **2001**, *80*, 157–240.

[2] G. A. Ardizzoia, S. Cenini, G. La Monica, N. Masciocchi, A. Maspero, M. Moret, *Inorg. Chem.* **1998**, *37*, 4284–4292.

[3] a) N. Masciocchi, M. Moret, P. Cairati, A. Sironi, G. A. Ardizzoia, G. La Monica, *J. Am. Chem. Soc.* **1994**, *116*, 7668–7676; b) H. V. R. Dias, S. A. Polach, Z. Wang, *J. Fluorine Chem.* **2000**, *103*, 163–169.

[4] a) R. G. Raptis, J. P. J. Fackler, *Inorg. Chem.* **1988**, *27*, 4179–4182; b) M. K. Ehlert, S. J. Rettig, A. Storr, R. C. Thompson, J. Trotter, *Can. J. Chem.* **1990**, *68*, 1444–1449; c) M. K. Ehlert, S. J. Rettig, A. Storr, R. C. Thompson, J. Trotter, *Can. J. Chem.* **1992**, *70*, 2161–2173; d) M. K. Ehlert, A. Storr, D. A. Summers, R. C. Thompson, *Can. J. Chem.* **1997**, *75*, 491–498; e) P. A. Angaridis, P. Baran, R. Boča, F. Cervantes-Lee, W. Haase, G. Mezei, R. G. Raptis, R. Werner, *Inorg. Chem.* **2002**, *41*, 2219–2228; f) R. Boča, L. Dlháň, G. Mezei, T. Ortiz-Pérez, R. G. Raptis, J. Telser, *Inorg. Chem.* **2003**, *42*, 5801–5803; g) M. Casarin, C. Corvaja, C. di Nicola, D. Falcomer, L. Franco, M. Monari, L. Pandolfo, C. Pettinari, F. Piccinelli, P. Tagliatesta, *Inorg. Chem.* **2004**, *43*, 5865–5876; h) G. Mezei, M. Rivera-Carrillo, R. G. Raptis, *Inorg. Chim. Acta* **2004**, *357*, 3721–3732; i) G. Mezei, R. G. Raptis, *Inorg. Chim. Acta* **2004**, *357*, 3279–3288; j) X. Liu, M. P. de Miranda, E. J. L. McInnes, C. A. Kilner, M. A. Halcrow, *Dalton Trans.* **2004**, 59–64.

[5] H. H. Murray, R. G. Raptis, J. P. J. Fackler, *Inorg. Chem.* **1988**, *27*, 26–33.

[6] F. Meyer, A. Jacobi, L. Zsolnai, *Chem. Ber./Receuil* **1997**, *130*, 1441–1447.

[7] a) B. Bovio, F. Bonati, G. Banditelli, *Inorg. Chim. Acta* **1984**, *87*, 25–33; b) R. G. Raptis, H. H. Murray, J. P. J. Fackler, *Acta Crystallogr. Sect. C* **1988**, *44*, 970–973; c) R. G. Raptis, J. P. J. Fackler, *Inorg. Chem.* **1990**, *29*, 5003–5006; d) S. J. Kim, S. H. Kang, K.-M. Park, H. Kim, W.-C. Zin, M.-G. Choi, K. Kim, *Chem. Mater.* **1998**, *10*, 1889–1893; e) J. Barberá, A. Elduque, R. Giménez, F. J. Lahoz, J. A. López, L. A. Oro, J. L. Serrano, *Inorg. Chem.* **1998**, *37*, 2960–2967; f) G. Yang, R. G. Raptis, *Inorg. Chem.* **2003**, *42*, 261–263; g) M. C. Torralba, P. Ovejero, M. J. Mayoral, M. Cano, J. A. Campo, J. V. Heras, E. Pinilla, M. R. Torres, *Helv. Chim. Acta* **2004**, *87*, 250–263.

[8] P. Baran, C. M. Marrero, S. Pérez, R. G. Raptis, *Chem. Commun.* **2002**, 1012–1013.

[9] K. Umakoshi, Y. Yamauchi, K. Nakamiya, T. Kojima, M. Yamasaki, H. Kawano, M. Onishi, *Inorg. Chem.* **2003**, *42*, 3907–3916.

[10] W. Burger, J. Strähle, *Z. Anorg. Allg. Chem.* **1985**, *529*, 111–117.

[11] a) A. C. Skapski, M. L. Smart, *J. Chem. Soc. Chem. Commun.* **1970**, 658–659; b) N. N. Lyalina, S. V. Dargina, A. N. Sobolev, T. M. Buslaeva, I. P. Romm, *Koord. Khim.* **1993**, *19*, 57–63; c) F. A. Cotton, S. Han, *Rev. Chim. Miner.* **1983**, *20*, 496–503.

[12] K. Umakoshi, T. Kojima, Y. H. Kim, M. Onishi, Y. Nakao, S. Sakaki, unpublished results.

[13] G. A. Ardizzoia, G. La Monica, S. Cenini, M. Moret, N. Masciocchi, *J. Chem. Soc. Dalton Trans.* **1996**, 1351–1357.

[14] J. Forniés, A. Martin, V. Sicilia, L. F. Martin, *Chem. Eur. J.* **2003**, *9*, 3427–3435.

[15] T. V. O'Halloran, S. J. Lippard, *Inorg. Chem.* **1989**, *28*, 1289–1295.

[16] W. Burger, J. Strähle, *Z. Anorg. Allg. Chem.* **1986**, *539*, 27–32.

[17] F. L. Wimmer, S. Wimmer, P. Castan, R. J. Puddephatt, *Inorg. Synth.* **1992**, *29*, 185–187.

[18] R. Usón, A. Laguna, M. Laguna, *Inorg. Synth.* **1989**, *26*, 85–91.

[19] S. Trofimenko, J. C. Calabrese, J. S. Thompson, *Inorg. Chem.* **1987**, *26*, 1507–1514.

[20] R. A. Jacobson, REQABS, version 1.1, Molecular Structure Corp., The Woodlands, TX, **1998**.

[21] A. Altomare, G. Cascarano, C. Giacovazzo, A. Guagliardi, M. C. Burla, G. Polidori, M. Camalli, *J. Appl. Crystallogr.* **1994**, *27*, 435–436.

[22] P. T. Beurskens, G. Admiraal, G. Beurskens, W. P. Bosman, R. de Gelder, R. Israel, J. M. M. Smits, The DIRDIF94 Program System, Crystallography Laboratory, University of Nijmegen, The Netherlands, **1994**.

[23] teXsan: Crystal Structure Analysis Package, Molecular Structure Corporation, The Woodlands, TX 77381, USA, **1999**.

[24] No significant broadening of the proton resonances was observed for **3b** and **4a** in their ^{1}H NMR spectra in $CDCl_3$ at −60 °C. We recently found that the isomerization of **4a** in [D_6]acetone is accelerated by addition of $Ag(CF_3SO_3)$ and the rate is affected by the concentration of coexisting Ag^I (Figure S5 and Table S1). The addition of Ag^I caused a slight downfield shift of proton resonances in the aromatic region without the appearance of new resonances corresponding to **3a** or other species (Figure S6). No significant broadening of the proton resonances was observed even at −40 °C for **4a** in the presence of two equivalents of Ag^I in [D_6]acetone. These observations indicate that, in the solution containing **4a** and Ag^I, the exchange process of Au^I and Ag^I is exceedingly faster than the others involved in the isomerization of **4a**. Further study is necessary to elucidate the mechanism of isomerization in detail.

Received: August 23, 2005
Revised: January 31, 2006
Published online: April 27, 2006

